Heterogeneous Catalysis

DOI: 10.1002/anie.201304610

# Mechanistic Role of Water on the Rate and Selectivity of Fischer–Tropsch Synthesis on Ruthenium Catalysts**

*David D. Hibbitts, Brett T. Loveless, Matthew Neurock,* and Enrique Iglesia**

Ru and Co catalyze Fischer–Tropsch synthesis (FTS) with high rates and $C_{5+}$ selectivities using stoichiometric synthesis gas and provide the preferred route to liquid fuels and petrochemicals.[1–3] O-atoms in CO are predominantly removed as $H_2O$,[2,3] a product that has been shown to increase,[2,4,5] decrease,[6] or not affect[3,7] turnover rates on Co-based catalysts, but which in all cases increases $C_{5+}$ and alkene selectivities on Co and Ru.[2,4,5]

$H_2O$ can inhibit rates by increasing O* coverages on Co;[6] such coverages require higher $H_2O/H_2$ ratios on Ru catalysts, rendering Ru catalysts stable even in aqueous media during FTS.[8] $H_2O$ promotion of FTS rates may reflect faster CO transport within $H_2O$-rich intrapore liquids when CO diffusion limits rates,[2] but $H_2O$ effects are observed even under conditions of strict kinetic control. $H_2O$-mediated rate enhancements may arise from higher densities of exposed metal atoms during FTS catalysis, possibly because chemisorbed carbon (C*) reacts with $H_2O$-derived species. Such a loss of binding sites, however, is inconsistent with CO* coverages (from infrared spectra) that do not depend on $H_2O$ pressure at levels that increased FTS rates by ca. 30%.[5] Stronger rate enhancements were reported for Co on large-pore supports, which require higher $H_2O$ pressures for intrapore condensation than small-pore supports, suggesting that a condensed $H_2O$ phase, which may exist within small-pore supports at very low CO conversions, may be required.[2,5,9] Here, Ru clusters on large-pore $SiO_2$ are used to measure rate and selectivity enhancements by $H_2O$, and density functional theory (DFT) calculations are used to examine the role of $H_2O$ as a co-catalyst in O–H formation steps in kinetically-relevant CO activation steps.

$H_2O$ pressures were varied by changing residence time (and CO conversion) or adding $H_2O$ to $H_2$–CO reactants.[5] CO consumption rates increased monotonically with increasing $H_2O$ pressure (up to 0.3 MPa $H_2O$; Figure 1), suggesting

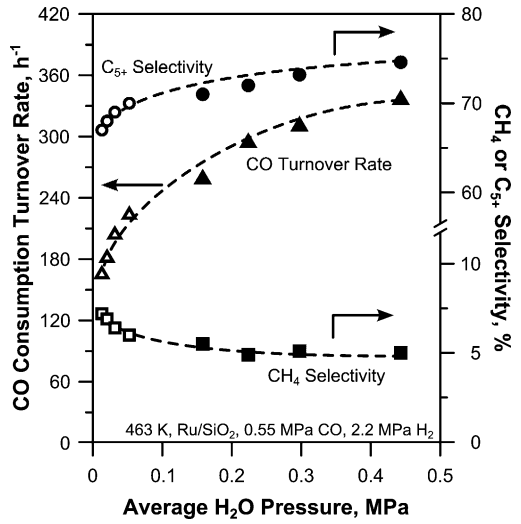


***Figure 1.*** CO consumption rate (△ or ▲), $CH_4$ selectivity (□ or ■), and $C_{5+}$ selectivity (○ or ●) as a function of $H_2O$ partial pressure on 5 wt% $Ru/SiO_2$ (463 K, 2.9 MPa, $H_2/CO = 4.5$). Open symbols: space velocity changes; closed symbols: $H_2O$-addition.

that $H_2O$ influences kinetically-relevant CO activation steps.[10] The weaker effects above 0.3 MPa $H_2O$ reflect co-adsorption of $H_2O$-derived species with CO*, H*, and their products. $H_2O$ decreased $CH_4$ selectivity and increased $C_{5+}$ selectivity (Figure 1), suggesting that $H_2O$-derived species increase monomer concentrations and/or their propagation rate constants.

Equation (1) describes the effects of $H_2$ and CO pressure on FTS rates at low and nearly constant $H_2O$ pressures on Co and Ru.[2,3,5,7,10,11]

$$r_{CO} = \frac{\alpha(CO)(H_2)}{[1 + K_{CO}(CO)]^2} \quad (1)$$

where (CO) and ($H_2$) are pressures. This equation indicates that kinetically-relevant transition states (TS) are bound at two vicinal Ru atoms and contain one CO and two H atoms. Direct CO* dissociation is irreversible and exhibits very high

[*] Dr. M. Neurock
Departments of Chemical Engineering and Chemistry
University of Virginia, Charlottesille, Virginia, 22904 (USA)
E-mail: neurock@virginia.edu
Homepage: http://www.che.virginia.edu/people/faculty/neurock.html
Dr. D. D. Hibbitts, Dr. B. T. Loveless, Dr. E. Iglesia
Department of Chemical and Biomolecular Engineering
University of California at Berkeley
Berkeley, California, 94720 (USA)
E-mail: iglesia@berkeley.edu
Homepage: http://iglesia.cchem.berkeley.edu/

[**] We thank BP for financial support through the BP Conversion Consortium (BP-XC$^2$) program as well as Drs. Glenn Sunley, Jay Labinger, Craig Plaisance, Corneliu Buda and the entire BP-XC$^2$ team for helpful discussions. We also wish to acknowledge the computational resources provided by the Molecular Science Computing Facility (MSCF) in the William R. Wiley Environmental Molecular Sciences Laboratory, a national scientific user facility sponsored by the U.S. Department of Energy, Office of Biological and Environmental Research at the Pacific Northwest National Laboratory.

Supporting information for this article is available on the WWW under http://dx.doi.org/10.1002/anie.201304610.

  

activation barriers, and the resulting rate equation is inconsistent with measured FTS rates, rendering such alternate routes implausible, as previously shown.[10]

Scheme 1 depicts three H-assisted CO activation routes consistent with Equation (1) and their respective lumped rate constants ($\alpha$). DFT-derived energies on CO*-covered $Ru_{201}$ clusters show that CO* and H* react to form HCO* in quasi-equilibrated steps (Step 3a), which then reacts irreversibly with H* to form *HCOH* (step 4a) (formyl route, Scheme 1),[10] as also found on Co and Fe surfaces.[3,11,12] Another route adds H* at the O-atom in CO* to form COH* (step 3b) in a quasi-equilibrated step that is followed by irreversible H* addition at the C-atom to form *HCOH* (step 4b) (hydroxymethylidyne route, Scheme 1).

1) $CO_{(g)} + * \rightleftharpoons CO^*$

2) $H_{2(g)} + 2^* \rightleftharpoons 2H^*$

***formyl route***

3a) $CO^* + H^* \rightleftharpoons HCO^* + *$

4a) $HCO^* + H^* \longrightarrow {}^*HCOH^*$ $\quad \alpha = K_{CO}K_{H_2}K_{3a}k_{4a}$

5a) $^*HCOH^* \longrightarrow CH^* + OH^*$

***hydroxymethylidyne route***

3b) $CO^* + H^* \rightleftharpoons COH^* + *$

4b) $COH^* + H^* \longrightarrow {}^*HCOH^*$ $\quad \alpha = K_{CO}K_{H_2}K_{3b}k_{4b}$

5b) $^*HCOH^* \longrightarrow CH^* + OH^*$

***carbon adatom route***

3c) $CO^* + H^* \rightleftharpoons COH^* + *$

4c) $COH^* + H^* \longrightarrow C^* + * + H_2O_{(g)}$ $\quad \alpha = K_{CO}K_{H_2}K_{3c}k_{4c}$

***Scheme 1.*** Hydrogen-assisted CO* activation during FTS. Quasi-equilibrated steps are denoted by reaction arrows overlaid with a circle.

The coverage dependence of CO* binding energies shows that $Ru_{201}$ clusters become saturated at 1.5 CO* per exposed Ru atom with supra-stoichiometric CO* species residing at corners and edges, and all CO* remaining in atop positions.[10] DFT-derived CO* binding energies ($-42\ kJ\,mol^{-1}$) and CO* entropies from Volmer gas 2-D models at these coverages give an adsorption free energy ($\Delta G_{ads} = 7.8\ kJ\,mol^{-1}$) similar to measured values ($2.2\ kJ\,mol^{-1}$).[10] These coverages and $Ru_{201}$ (111) terraces are used in all energy calculations (see Experimental Section)[10] and reflect the active sites involved in FTS.[10,13]

At high CO* coverages, Equation (1) becomes:

$$r_{CO} = \frac{K_{H_2}K_3k_4(H_2)}{K_{CO}(CO)} \qquad (2)$$

and effective barriers reflect energy differences between kinetically-relevant transition states (TS) and reactant states:

$$\Delta H_{eff} = -Q_{CO} + Q_{H_2} + \Delta H_{Rxn,3} + \Delta H_{Act,4} \qquad (3)$$

Here, steps 3 and 4 refer to those in Scheme 1 for each H-assisted CO activation sequence. In terms of the energies of the species involved, Equation (3) becomes [derivation in Supporting Information (SI), Eqs. (S3)–(S5)]:

$$\Delta H_{eff} = H_{TS_i^{**}} - \left(H_{CO^*} - H_{CO(g)}\right) - H_{CO^*} - \frac{n}{2}H_{H_2(g)} \qquad (4)$$

where $n$ is the number of H-atoms in the TS of step $i$.

Figure 2 shows DFT-derived reaction and activation energies for the formyl and hydroxymethylidyne routes. The HCO* formation barrier is $93\ kJ\,mol^{-1}$, while its reverse barrier ($30\ kJ\,mol^{-1}$) is much smaller than for its reaction with H* to form *HCOH* ($95\ kJ\,mol^{-1}$), indicating that HCO* formation is quasi-equilibrated. HCO* dissociation to form CH* and O* has a barrier of $155\ kJ\,mol^{-1}$,[10] which is much larger than H*-addition to HCO* to form *HCOH* ($95\ kJ\,mol^{-1}$). *HCOH* decomposes to HCO* and H* with a much larger barrier ($86\ kJ\,mol^{-1}$) than to CH* and OH* ($43\ kJ\,mol^{-1}$), indicating that *HCOH* formation is irreversible. It forms CH* and OH* species that react in subsequent kinetically-irrelevant steps to form the hydrocarbon and $H_2O$ products of FTS. The effective barrier for this formyl route is $193\ kJ\,mol^{-1}$ [Eq. (4)], which is much smaller than those for routes involving unassisted CO* dissociation ($322\ kJ\,mol^{-1}$).[10]

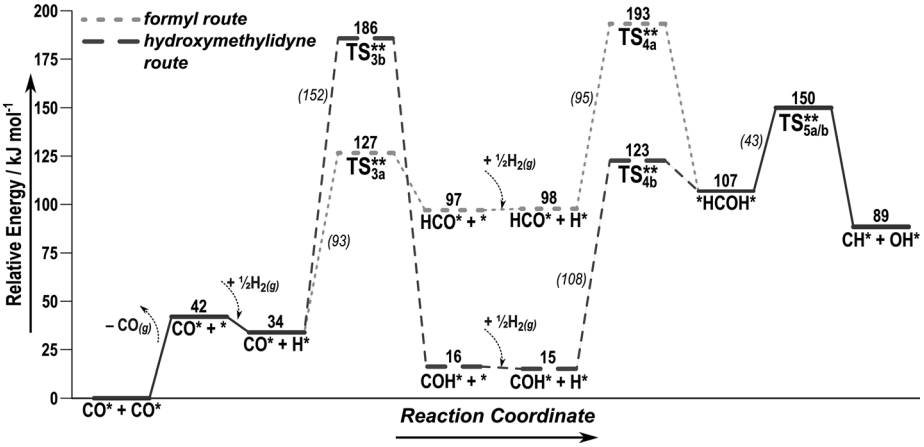


***Figure 2.*** Reaction coordinate diagrams for the two H*-assisted CO activation mechanisms in Scheme 1. Intrinsic activation barriers are in italics and effective barriers (with respect to CO*-covered $Ru_{201}$ particles; [Eq. (4)]) are in bold.

The barrier for H* addition to the O-atom in CO* (to form COH*; $152\ kJ\,mol^{-1}$) is larger than for the addition at the C-atom ($93\ kJ\,mol^{-1}$). COH* undergoes subsequent H*-addition to form *HCOH*, which forms CH* and OH*, as in the formyl route. In this route, COH* formation has the largest effective barrier [$186\ kJ\,mol^{-1}$, Figure 2, Eq. (4)] and

  

becomes the kinetically-relevant step, leading to the rate equation:

$$r_{CO} = \frac{k_{3b} K_{CO} K_{H_2}^{0.5} (CO)(H_2)^{0.5}}{[1 + K_{CO}(CO)]^2} \quad (5)$$

inconsistent with the measured first-order $H_2$ dependence of FTS rates, as also found on Co surfaces.[3]

$H_2O$-mediated rate enhancements require changes in the dynamics or identity of kinetically-relevant steps. Any enthalpic stabilization of relevant transition states must overcome concomitant entropy losses from hindered mobility of any $H_2O$ molecules involved. Measured effects of $H_2O$ on FTS rates can be described by Equation (6), a modified version of Equation (1). This equation contains a numerator term that accounts for the promotion of FTS rates by $H_2O$ and denominator terms for co-adsorption of $H_2O$-derived species formed in quasi-equilibrated steps [$H_2O$*, OH*, O*, Eqs. (7)–(9)].

$$r_{CO} = \frac{\alpha(CO)(H_2) + \beta(CO)(H_2)(H_2O)}{[1 + K_{CO}(CO) + K_{H_2O}(H_2O) + K_{OH}(H_2O)(H_2)^{-0.5} + K_O(H_2O)(H_2)^{-1}]^2} \quad (6)$$

$$H_2O + * \xrightleftharpoons{K_{H_2O}} H_2O^* \quad (7)$$

$$H_2O + * \xrightleftharpoons{K_{OH}} OH^* + {}^1/_2H_2 \quad (8)$$

$$H_2O + * \xrightleftharpoons{K_O} O^* + H_2 \quad (9)$$

The parity plot in Figure 3 shows that Equation (6) accurately describes all rate data in Figure 1, as well as previously reported data.[10] The relative contributions from O*, OH* and $H_2O$* coverages cannot be inferred from these data as determined by a sensitivity analysis (Table S2, Figure S10, SI), but DFT-derived free energies (Figure S12, SI) show that $H_2O$* is the preferred $H_2O$-derived adsorbate on Ru. The values of $\alpha$ ($0.66 \pm 0.11$) and $K_{CO}$ ($6.2 \pm 0.7$) shown in Table 1 agree with values reported previously[10] at low $H_2O$ pressures ($0.58 \pm 0.08$ and $5.6 \pm 0.6$, respectively).

***Table 1:*** Fitted lumped rate constants $\alpha$ and $\beta$, and CO and $H_2O$ adsorption constants ($K_{CO}$ and $K_{H_2O}$) for FTS on $SiO_2$-supported 7 nm Ru clusters (463 K).

| | $\alpha$ [mol $s^{-1}$ mol $Ru^{-1}$ $MPa^{-2}$] | $\beta$ [mol $s^{1}$ mol $Ru^{-1}$ $MPa^{-3}$] | $K_{CO}$ [$MPa^{-1}$] | $K_{H_2O}$ [$MPa^{-1}$] | $K_{OH}$ [$MPa^{-0.5}$] | $K_O$ |
|---|---|---|---|---|---|---|
| Ref. [10a] also on 7 nm Ru | $0.58 \pm 0.08$ | – | $5.6 \pm 0.6$ | – | – | – |
| This work | $0.66 \pm 0.11$ | $4.72 \pm 1.1$ | $6.2 \pm 0.7$ | 0–3.1 | 0–3.9 | 0–5.1 |

The $H_2O$ enhancement factor ($\chi$):

$$\chi = \frac{\beta(H_2O)}{\alpha} = \exp\left(\frac{-\Delta(\Delta G_{eff})}{RT}\right) \quad (10)$$

is defined as the ratio of the two numerator terms from Equation (6). The fitted values of $\alpha$ and $\beta$ (Table 1) gives a $\chi$ of $7 \pm 3$ at 1 bar $H_2O$ and 463 K, which corresponds to a difference in free energy barriers ($\Delta(\Delta G_{eff})$) between $H_2O$-mediated and anhydrous routes of $-8 \pm 2$ kJ $mol^{-1}$.

$H_2O$ may influence formyl routes 1) as a H-source ($H_2O$* reaction with HCO* to form *HCOH* and OH*), 2) as a "solvent" to stabilize the TS for H-addition at the O-atom in HCO* (through H-bonding with incipient O–H bonds), or 3) as a H-shuttling agent (as a $H_2O$ molecule or extended phase) for H* transfer to the O-atom in HCO*, as shown in Scheme 2.

Figure 4 shows DFT-derived energies for $H_2O$-mediated hydroxymethylidyne route, for which the effective barriers are:

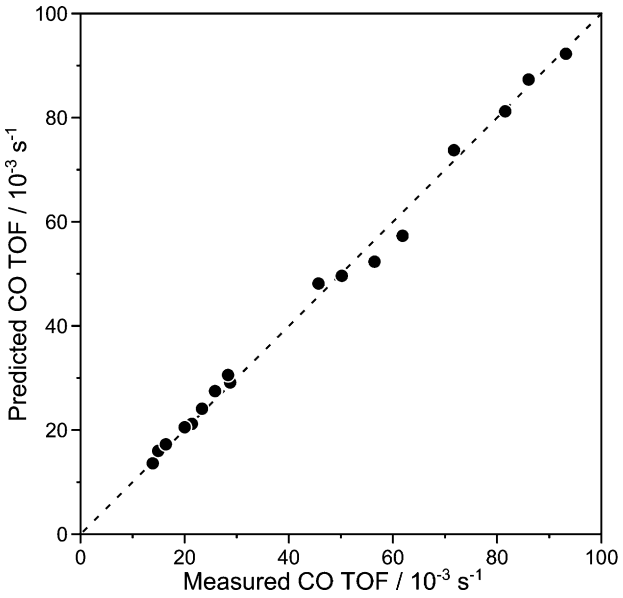


***Figure 3.*** Measured and predicted CO consumption turnover rates (predictions from Equation (9) and parameters in Table 1.)

***formyl route without $H_2O$***

3a) CO* + H* ⇌ HCO* + *

4a) HCO* + H* → *HCOH*

5a) *HCOH* → CH* + OH*

***formyl route with $H_2O$ as H-source***

3d) CO* + H* ⇌ HCO* + *

4d) $H_2O_{(g)}$ + * ⇌ $H_2O$*

5d) HCO* + $H_2O$* + * → CH* + 2OH*

***formyl route with $H_2O$ as solvent or H-shuttle***

3e) $H_2O_{(g)}$ + CO* ⇌ CO*···$H_2O$

4e) CO*···$H_2O$ + H* ⇌ HCO*···$H_2O$ + *

5e) HCO*···$H_2O$ + H* → *HCOH*···$H_2O$

6e) *HCOH*···$H_2O$ → CH* + OH*···$H_2O$

***hydroxymethylene route with $H_2O$ as solvent or H-shuttle***

3f) $H_2O_{(g)}$ + CO* ⇌ CO*···$H_2O$

4f) CO*···$H_2O$ + H* ⇌ COH*···$H_2O$ + *

5f) COH*···$H_2O$ + H* ⇌ *HCOH*···$H_2O$

6f) *HCOH*···$H_2O$ → CH* + OH*···$H_2O$

***Scheme 2.*** $H_2O$-mediated *HCOH* formation via formyl or hydroxymethylidyne intermediates. Quasi-equilibrated steps are denoted by reaction arrows overlaid with a circle.

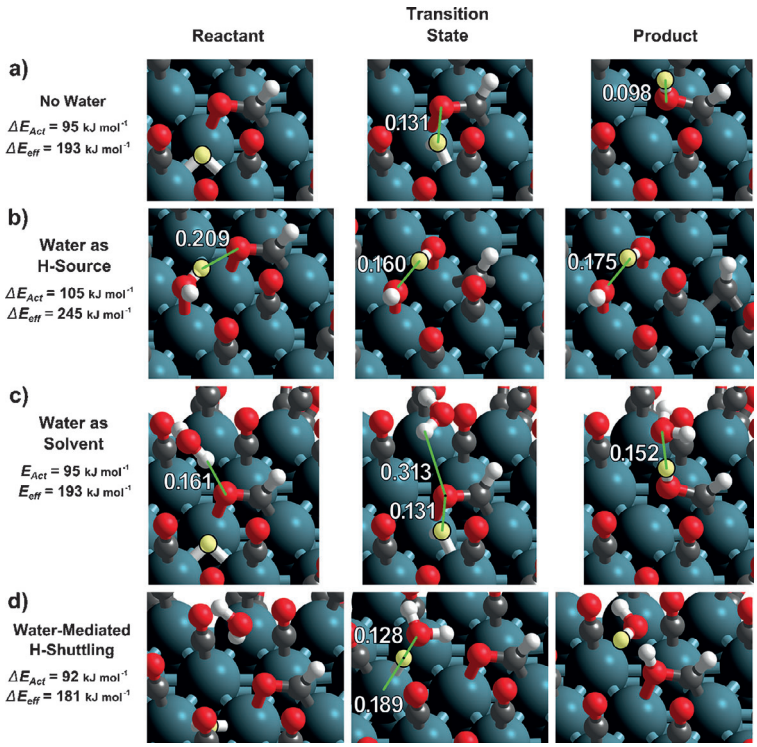


***Figure 4.*** DFT-derived reactant, TS, and product structures in *HCOH* formation of the formyl route a) direct H*-addition, b) $H_2O$ as a H-source, c) $H_2O$ as a solvent, and d) $H_2O$ as a H-shuttle (the transferred H-atom is highlighted and distances are in nm).

$$\Delta H_{\mathrm{eff}} = H_{\mathrm{TS_i^{**}}} - \left(H_{\mathrm{CO^*}} - H_{\mathrm{CO(g)}}\right) - H_{\mathrm{CO^*}} - \frac{n}{2}H_{\mathrm{H_2(g)}} - H_{\mathrm{H_2O(g)}} \qquad (11)$$

These barriers include, in contrast with those for the anhydrous case [Eq. (5)], energies for the $H_2O$-containing transition state and its $H_2O$(g) precursor (Scheme 2, Steps 3e/f). $H_2O$ as a H-source, solvent, or H-shuttle can increase (by 52 kJ mol$^{-1}$), have no effect, or slightly decrease (by 12 kJ mol$^{-1}$), respectively, the effective barriers in the formyl route that prevails in the absence of $H_2O$ (Figure 4). Concomitant entropy losses upon $H_2O$ fixation, however, make activation free energies larger than for anhydrous routes, even for H-shutting. We conclude that these $H_2O$ mediated routes do not account for the measured rate enhancements.

Hydroxymethylidyne routes are disfavored in the absence of water, but may become the preferred path through the influence of water. $H_2O$-mediated H-shuttling leads to COH* formation activation energies [111 kJ mol$^{-1}$, Figure 5, Figure 6a, Eq. (11)] much smaller than for H* addition without $H_2O$ [186 kJ mol$^{-1}$, Figure 2, Eq. (4)]. H-shuttling involves electron transfer from H* to Ru as H* interacts with $H_2O$ to form $H_3O^{\delta+}$ species, which protonates CO* in a manner reminiscent of proton coupled electron transfer steps in aqueous media[14] and in $H_2O$-aided H-diffusion.[15] Bader charges[16] indicate that $\delta$ is +0.87. *HCOH* dissociation barriers (129 kJ mol$^{-1}$) are larger than for COH* dissociation (111 kJ mol$^{-1}$), consistent with quasi-equilibrated COH* formation through $H_2O$-assisted H-shuttling [Eq. (S26), SI]. The effective barrier for $H_2O$-mediated hydroxymethylidyne routes (129 kJ mol$^{-1}$) is much smaller than for $H_2O$-mediated formyl routes (181 kJ mol$^{-1}$), indicating that $H_2O$ mediation opens a C–O activation route absent at low $H_2O$ concentrations. In this route, the kinetically-relevant activation of C–O bonds in *HCOH* (to form CH* and OH*) proceeds though a TS that involves two H atoms and a CO-derived species, which is consistent with reported FTS rate equations on Co and Ru catalysts[2,3,5,7,10,11] [Eq. (1)].

Rearranging Equation (10) with the $\alpha$ and $\beta$ values for the full FTS rate equation [Eq. (6)] gives:

$$\alpha = K_{\mathrm{CO}}K_{\mathrm{H_2}}K_{\mathrm{3a}}K_{\mathrm{4a}}k_{\mathrm{5a}} \qquad (12)$$

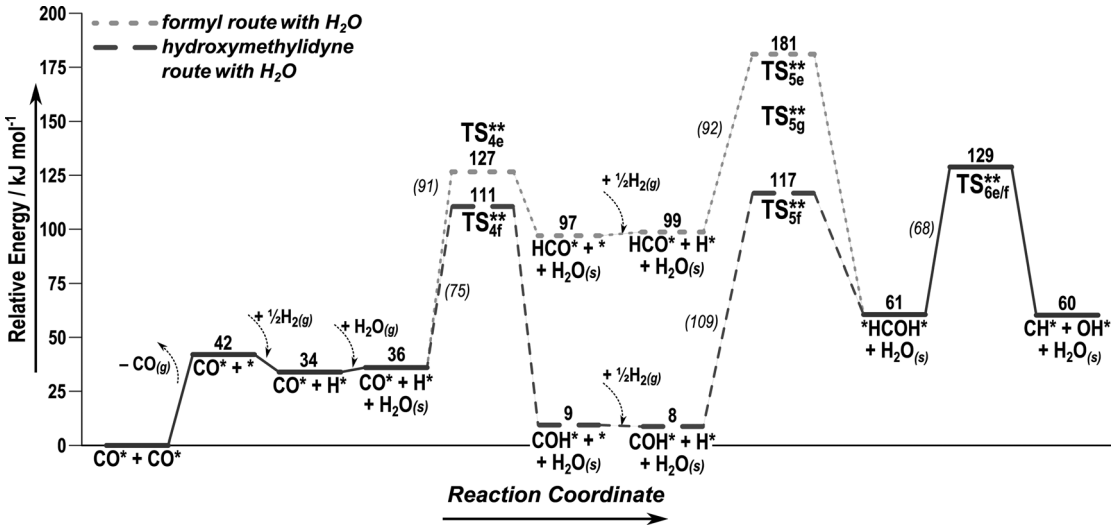


***Figure 5.*** Reaction coordinate diagrams for $H_2O$-mediated formyl and hydroxymethylidyne routes in the presence of $H_2O$. Intrinsic activation barriers are in italics and effective barriers (with respect to CO*-covered $Ru_{201}$ particles; [Eq. (11)]) are in bold.

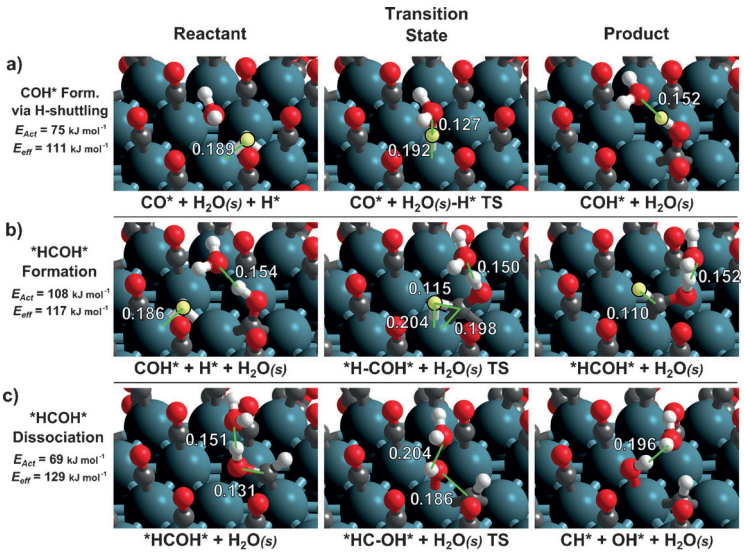


***Figure 6.*** DFT-derived reactant, TS and product structures for the $H_2O$-mediated hydroxymethylidyne route (the transferred H-atom is highlighted and distances are in nm).

$$\beta = K_{CO}K_{H_2}K_{3f}K_{4f}K_{5f}k_{6f} \tag{13}$$

$$\chi = \frac{K_{3f}K_{4f}K_{5f}k_{6f}(H_2O)}{K_{3a}K_{4a}k_{5a}} = \exp\left(\frac{-\Delta(\Delta G_{eff})}{RT}\right) \tag{14}$$

The measured free energy difference between the anhydrous and $H_2O$-mediated terms in Equation 10 ($\Delta(\Delta G_{eff}) = -8 \pm 2$ kJ mol$^{-1}$) is related to their respective differences in enthalpy ($\Delta(\Delta H_{eff})$) and entropy ($\Delta(\Delta S_{eff})$):

$$\Delta(\Delta G_{eff}) = \Delta(\Delta H_{eff}) - T(\Delta(\Delta S_{eff})) \tag{15}$$

The $\Delta(\Delta H_{eff})$ between the $H_2O$-mediated hydroxymethylidyne route ($\Delta H_{eff} = 129$ kJ mol$^{-1}$, Figure 4) and the anhydrous formyl route ($\Delta H_{eff} = 193$ kJ mol$^{-1}$, Figure 2) is $-64$ kJ mol$^{-1}$, and is related to the difference in enthalpy of the $H_2O$-mediated kinetically-relevant transition state $\left(H^{\pm}_{H_2O-med.}\right)$ and the anhydrous kinetically relevant transition state $\left(H^{\pm}_{Anh.}\right)$ and gas-phase water.

$$\Delta(\Delta H_{eff}) = H^{\pm}_{H_2O-med.} - H^{\pm}_{Anh.} - H_{H_2O(g)} \tag{16}$$

The value of $\Delta(\Delta S_{eff})$ reflects the entropy loss caused by the "fixation" of a $H_2O$ molecule at the hydroxymethylene TS. Assuming that the vibrational entropy of the two transition states are similar, the majority of this loss can be estimated as the $\Delta S$ upon $H_2O$ physisorption which has been estimated from adsorption isotherms [Eq. (S27)–(S30)] as $134 \pm 10$ J mol$^{-1}$ K$^{-1}$.[17]

$$\Delta(\Delta S_{eff}) = S^{\pm}_{H_2O-med.} - S^{\pm}_{Anh.} - S_{H_2O(g)} \approx S_{H_2O,Phys.} \tag{17}$$

Substituting $\Delta(\Delta H_{eff})$ and $\Delta(\Delta S_{eff})$ values into Equation (15) gives a $\Delta(\Delta G_{eff})$ estimate of $-2 \pm 5$ kJ mol$^{-1}$ at 463 K and 1 bar, which lie within the uncertainty range of the measured enhancement factor ($-8 \pm 2$ kJ mol$^{-1}$).

$H_2O$ also increases the chain length of FTS products (Figure 1 and Ref. [2,4]), indicating that it promotes chain growth without commensurate effects on chain termination. The precise nature of chain growth pathways and the monomers involved remains controversial, a subject that we address in a later study.[2,3] We illustrate here two plausible effects of $H_2O$ on chain growth, based on the experimental and theoretical evidence presented above for $H_2O$ mediation of H-assisted C–O bond cleavage.

C–C bonds may form by alkyl chain reactions with "activated" $C_1$ species [Eq. (18)] or by sequential reactions of such alkyls with CO* and H* to form hydroxyalkylidenes that dissociate to form alkylidynes and OH* [Eq. (19)]. CO* may also react with alkylidynes and alkylidenes,[18] which hydrogenate to form hydroxyalkylidenes; our simulations[19] show, however, that CH* and $CH_2$* hydrogenation barriers are much smaller than for their reactions with CO*, indicating that they would convert to alkyls before further chain growth. Termination occurs either by β-H elimination to form terminal alkenes [Eq. (20)] or H*-addition to form *n*-alkanes [Eq. (21)].[3]

$$C_nH_{2n+1}{}^* + CH_x{}^* \rightarrow C_{n+1}H_{2n+1+x}{}^* + * \tag{18}$$

$$C_nH_{2n+1}{}^* + CO^* + H^* \rightarrow {}^*C_nH_{2n+1}COH^* + * \rightarrow C_nH_{2n+1}C^* + OH^* + * \tag{19}$$

$$C_nH_{2n+1}{}^* + * \rightarrow C_nH_{2n}{}^* + H^* \tag{20}$$

$$C_nH_{2n+1}{}^* + H^* \rightarrow C_nH_{2n+2}{}^* + * \tag{21}$$

$H_2O$ increases the rate of formation of activated $C_1$ species and, in doing so, the steady-state $CH_x$* coverages and the chain growth rate [through Eq. (18)], without concomitant effects on termination rates.[20] C–C bond formations by reactions in which CO* reacts with an alkyl chain and H* [Eq. (19)] are analogous to CO* activation in which CO* reacts with two H* as the chemical nature of an alkyl species is similar to that of H* indicating that $H_2O$ would decrease activation barriers for chain growth via Equation (19) by similar H-shuttling mediation, leading to heavier products and higher $C_{5+}$ selectivities, as found experimentally.

We conclude that $H_2O$, whether indigenous or co-fed, increases CO activation rates on Ru-based catalysts in a manner consistent with the involvement of $H_2O$-mediated H-transfer routes and competitive adsorption of $H_2O$-derived intermediates [Eq. (9)]. DFT-derived reaction and activation energies indicate that $H_2O$ mediates the kinetically-relevant H-transfer required for O–H bond formation in pathways involving *HCOH* intermediates and increases chain growth probabilities by increasing the rate of monomer formation when growth occurs via $CH_x$* or the rate constant for chain growth when CO* is the monomer. $H_2O$ can act as a co-catalyst in FTS reactions in doing so, as previously observed in metal-catalyzed hydrogenations in protic media.[14,15] The kinetic resemblance among Ru and Co catalysts[2,3,5,6,10] suggest that similar conclusions about $H_2O$-mediated routes

  

apply to FTS catalysis on Co, on which FTS rates and product chain length also increase with increasing $H_2O$ pressure.[2,4,5]

## Experimental Section

A 5 wt% $Ru/SiO_2$ catalyst was prepared as reported elsewhere.[10,21] The Ru particle size was found to be 7 nm[10] and the $SiO_2$ support (PQ Corp. CS-2133, 350 $m^2 g^{-1}$) has an average pore diameter of 13 nm.[5] FTS rates and selectivities were measured in an isothermal ($\pm 2$ K) fixed bed stainless steel reactor (I.D. = 1 cm) with a catalyst bed (15 cm) consisting of 5 wt% $Ru/SiO_2$ (0.9 g) catalyst and $SiO_2$ diluent (3.5 g). The catalyst and diluent mixture was heated to 673 K at 2 K $min^{-1}$ in flowing $H_2$ and holding for 10 h at ambient pressures prior to exposure of the catalyst to reactants. Reported rates and selectivities, determined via analysis of the reaction effluent by online gas chromatography as reported elsewhere,[10] correspond to steady-state values obtained after 24 h on-stream. DFT calculations were performed as previously reported[10] on a 201-atom Ru nanoparticle at a CO* coverage of 1.55 ML using the VASP software package with ultra-soft pseudopotentials and the Perdew-Wang 91 form of the generalized gradient approximation.[22]

Received: May 28, 2013
Revised: August 5, 2013
Published online: October 2, 2013

**Keywords:** density functional calculations · Fischer–Tropsch synthesis · heterogeneous catalysis · hydrogenation · kinetics

[1] F. Fischer, H. Tropsch, *Brennst.-Chem.* **1926**, *7*, 97.
[2] E. Iglesia, *Appl. Catal. A* **1997**, *161*, 59.
[3] a) M. Vannice, *Catal. Rev. Sci. Eng.* **1976**, *14*, 153; b) E. Iglesia, S. Reyes, R. Madon, S. Soled, *Adv. Catal.* **1993**, *39*, 221; c) M. Ojeda, R. Nabar, A. Nilekar, A. Ishikawa, M. Mavrikakis, E. Iglesia, *J. Catal.* **2010**, *272*, 287.
[4] a) H. Schulz, E. vein Steen, M. Claeys, *Stud. Surf. Sci. Catal.* **1994**, *81*, 455; b) H. Schulz, M. Claeys, S. Harms, *Stud. Surf. Sci. Catal.* **1997**, *107*, 193; c) C. Kim (Exxon), US 0355218, **1990**; d) C. Kim (Exxon), US 5227407, **1993**; e) J. Li, G. Jacobs, T. Das, Y. Zhang, B. Davis, *Appl. Catal. A* **2002**, *236*, 67.
[5] S. Krishnamoorthy, M. Tu, M. Ojeda, D. Pinna, E. Iglesia, *J. Catal.* **2002**, *211*, 422.
[6] a) F. Gottschalk, R. Copperthfvaite, M. van der Riet, G. Hutchings, *Appl. Catal.* **1988**, *38*, 103; b) P. van Berge, J. van de Loosdrecht, S. Barradas, A. van der Kraan, *Catal. Today* **2000**, *58*, 321; c) D. Schanke, A. Hilmen, E. Bergene, K. Kinnari, E. Rytter, E. Adnanes, A. Holmen, *Catal. Lett.* **1995**, *34*, 269; d) A. Hilmen, D. Schanke, K. Hanssen, A. Holmen, *Appl. Catal. A* **1999**, *186*, 169.
[7] a) I. Yates, C. Satterfield, *Energy Fuels* **1991**, *5*, 168–173; b) B. Jager, R. Espinoza, *Catal. Today* **1995**, *23*, 17.
[8] C. Xiao, Z. Cai, T. Wang, Y. Kou, N. Yan, *Angew. Chem.* **2008**, *120*, 758; *Angew. Chem. Int. Ed.* **2008**, *47*, 746.
[9] A. Dalai, T. Das, K. Chaudhari, G. Jacobs, B. Davis, *Appl. Catal. A* **2005**, *289*, 135.
[10] a) B. Loveless, C. Buda, M. Neurock, E. Iglesia, *J. Am. Chem. Soc.* **2013**, *135*, 6107; b) B. Loveless, E. Iglesia, *J. Catal.* **2013**, submitted.
[11] M. Ojeda, A. Li, R. Nabar, M. Mavrikakis, E. Iglesia, *J. Phys. Chem. C* **2010**, *114*, 19761.
[12] a) S. Shetty, A. Jansen, R. van Santen, *J. Am. Chem. Soc.* **2009**, *131*, 12874; b) O. Inderwildi, S. Jenkins, D. King, *J. Phys. Chem. C* **2008**, *112*, 1305; c) M. Zhuo, K. Tan, A. Borgna, M. Saeys, *J. Phys. Chem. C* **2009**, *113*, 8357; d) M. Elahifard, M. Jigato, J. Niemantsverdriet, *ChemPhysChem* **2012**, *13*, 89; e) M. Andersson, T. Bligaard, A. Kustov, K. Larsen, J. Greeley, T. Johannessen, C. Christensen, J. Nørskov, *J. Catal.* **2006**, *239*, 501.
[13] a) J. den Breejen, P. Radstake, G. Bezemer, J. Bitter, V. Frøseth, A. Holmen, K. de Jong, *J. Am. Chem. Soc.* **2009**, *131*, 7197; b) J. den Breejen, J. Sietsma, H. Freidrich, J. Bitter, K. de Jong, *J. Catal.* **2010**, *270*, 146.
[14] a) D. Cao, G. Lu, A. Wieckowski, S. Wasileski, M. Neurock, *J. Phys. Chem. B* **2005**, *109*, 11622; b) S. Desai, M. Neurock, *Electrochim. Acta* **2003**, *48*, 3759; c) S. Desai, V. Pallassana, M. Neurock, *J. Phys. Chem. B* **2001**, *105*, 9171; d) M. Janik, C. Taylor, M. Neurock, *J. Electrochem. Soc.* **2009**, *156*, B126; e) M. Ide, B. Hao, M. Neurock, R. Davis, *ACS Catal.* **2012**, *2*, 671; f) Y. Zhao, Y. Yang, C. Mims, C. Peden, J. Li, D. Mei, *J. Catal.* **2011**, *281*, 199; g) C. Michel, F. Auneau, F. Delbecq, P. Sautet, *ACS Catal.* **2011**, *1*, 1430.
[15] a) M. Janik, R. Davis, M. Neurock, *J. Am. Chem. Soc.* **2005**, *127*, 5238; b) M. Janik, B. Bardin, R. Davis, M. Neurock, *J. Phys. Chem. C* **2006**, *110*, 4170; c) L. Merte, G. Peng, R. Bechstein, F. Rieboldt, C. Farberow, L. Grabow, W. Kudernatsch, S. Wendt, E. Laegsgaard, M. Mavrikakis, F. Besenbacher, *Science* **2012**, *336*, 889.
[16] G. Henkelman, A. Arnaldsson, J. Jónsson, *Comput. Mater. Sci.* **2006**, *36*, 354.
[17] M. Nagao, *J. Phys. Chem.* **1971**, *75*, 3822.
[18] a) O. Inderwildi, D. King, S. Jenkins, *Phys. Chem. Chem. Phys.* **2009**, *11*, 11110; b) M. Zhuo, A. Borgna, M. Saeys, *J. Catal.* **2013**, *297*, 217.
[19] C. Buda, T. Lawlor, D. Hibbitts, M. Neurock, unpublished results.
[20] C. Bertole, C. Mims, G. Kiss, *J. Catal.* **2002**, *210*, 84.
[21] S. Soled, A. Malek, S. Miseo, J. Baumgartner, C. Kliewer, M. Afeworki, P. Stevens, *Stud. Surf. Sci. Catal.* **2006**, *162*, 103.
[22] a) G. Kresse, J. Hafner, *Phys. Rev. B* **1993**, *47*, 558; b) D. Vanderbilt, *Phys. Rev. B* **1985**, *32*, 8412; c) J. Perdew, J. Chevary, S. Vosko, K. Jackson, M. Pederson, D. Singh, C. Fiolhais, *Phys. Rev. B* **1992**, *46*, 6671.

  